



Evolution of microstructures and properties of magnesium alloy weldments produced with CO₂ laser process

Chun-Ming Lin^{a,b,*}, Hsien-Lung Tsai^a, Chang-Lin Lee^a, Di-Shiang Chou^b, Jen-Ching Huang^c

^a Department of Mechanical Engineering, National Taiwan University of Science and Technology, Taipei, 10673, Taiwan, ROC

^b Department of Geosciences, National Taiwan University, Taipei, 106, Taiwan, ROC

^c Department of Mechanical engineering, Tunghan University, ShenKeng 22202, Taiwan, ROC

ARTICLE INFO

Article history:

Received 13 July 2011

Received in revised form 5 February 2012

Accepted 10 March 2012

Available online 7 April 2012

Keywords:

Mechanical characterization

Magnesium alloys

Welding

Fracture

ABSTRACT

This study investigates the microstructure, hardness, and tensile strength of AZ31 and AZ61 magnesium alloy weldments fabricated in a CO₂ laser welding process. Results show that the AZ31 weldment contains cellular grains within the fusion zone (FZ). By contrast, the FZ of the AZ61 weldment contains a mixture of cellular and columnar grains and the PMZ contains bulk grains. It can be inferred that differences in the aluminum content of the two alloys (i.e., AZ31: 2.66 wt%; AZ61: 5.25 wt%) results in different supercooling rates and solid grain structures. The aluminum content also influences the formation of precipitates and defects in the weld bead during solidification, due to altered cooling rates resulting from thermal effects triggered by the growth of the precipitation phase. In particular, the AZ61 weldment exhibits high microporosity in the PMZ region with micropores or voids at the bottom of the weld bead. It is speculated that these defects are the result of liquation cracking. CO₂ laser welding has been shown to increase the hardness of both magnesium alloys, with the maximum hardness occurring in the FZ of both weldments due to grain refining. The AZ61 weldment has the higher hardness of the two, due to increased grain refinement resulting from higher Al content. For both weldments, the ultimate tensile strength (UTS) decreases following CO₂ laser welding. However, no significant difference was noted between the UTS of the two weldments, suggesting that tensile strength is insensitive to the Al content of the magnesium alloys. By contrast, the uniform elongation increases with an increase in Al content in these alloys, indicating that the uniform elongation of the two weldments is sensitive to the Al content. Finally, the two weldments exhibit different fracture behavior resulting from differences in the size of the supersaturated precipitates formed in the two specimens and the presence of micropores and voids in the AZ61 specimen.

© 2012 Elsevier B.V. All rights reserved.

1. Introduction

Light alloy systems, comprising mainly aluminum, titanium, and magnesium alloys [1–4], have found wide application in the transportation, 3C, construction, and machinery industries in recent years. As consumer demand for energy efficiency and environmental protection continues to grow, the application of lightweight, environmentally friendly alloy systems will continue to expand. Magnesium alloy systems have an exceptionally low specific weight [5–8]; however, they are highly susceptible to oxidation and have a low melting point, which invariably results in the formation of defects when soldered or welded [9,10]. As a result, the

formability of such systems using traditional techniques is somewhat limited. To overcome this problem, a variety of enhanced methods for the bonding of magnesium alloy systems have been proposed, including friction stir welding [11–13], tungsten inert gas welding with added flux [14], laser/electron beam welding [2,15,16], and vacuum diffusion bonding [17,18]. In particular, laser welding has a number of important advantages, including low heat input and rapid welding speed (resulting in reduced thermal deformation), and the potential for automation. However, research into the laser welding of magnesium alloy systems is still in its early stages, and thus relevant studies are scant [15,16]. However, researchers have investigated the microstructure and properties of various magnesium alloy weldments fabricated using a laser process under various welding parameters [15,16,19,20]. Results indicate that a number of these welding parameters clearly influence the geometry of joints. Increasing the heat input increases the width of the weld, while differences in the depth of penetration between the top and bottom of the weld are reduced. Note

* Corresponding author at: Department of Mechanical Engineering, National Taiwan University of Science and Technology 43, Keelung Road, Section 4, Taipei, 10673, Taiwan, ROC. Tel.: +886 2 2737 7304; fax: +886 2 2737 6460.

E-mail address: D9503503@mail.ntust.edu.tw (C.-M. Lin).

that a higher weld power results in higher energy density, leading to a significant increase in weld penetration as well as various thermal effects that influence the supercooling rate, the formation of precipitates, and the solidified grain structure of the laser weldments [19,20]. In [19], it was reported how heat input influences metallurgical changes and it has been demonstrated that grain morphology, average grain size, and precipitate phase have a considerable influence on weldment performance. A few related studies have demonstrated that CO₂ laser welding induces liquation cracking in aluminum alloy systems [21–23]. Although the origins of this phenomenon were not examined in depth, it has been speculated that a portion of the grain boundary surrounding the welding rod forms a melting zone, resulting in uneven solidification of the solid–liquid interface. This prevents the molten metal from flowing freely to the surrounding melting zones, leading to the formation of cracks due to contractile tension. This study investigates the microstructure, hardness, and tensile strength of two magnesium alloy weldments with different aluminum contents, fabricated using a CO₂ laser welding process. Our investigation focuses specifically on the influence of aluminum content on the solidified grain structure, the formation of welding defects, the precipitation of supersaturated phases, the formation and growth of liquation cracking, and the mechanical properties of the weldments.

2. Materials and methods

2.1. Experimental materials

Welding trials were performed using AZ31 and AZ61 magnesium alloy plates with dimensions of 70 mm × 50 mm × 2 mm. The chemical composition of the plates was as follows: AZ31, 95.98Mg–2.66Al–0.89Zn–0.12Mn–0.09Si–0.01Cu (wt%); and AZ61, 93.83Mg–5.25Al–0.56Zn–0.04Mn–0.03Si–0.02Cu (wt%).

2.2. Experimental procedure

Prior to the welding tests, the plates were cleaned with emery paper to remove the oxidized layer. The edges of the plates were then mechanically cleaned with abrasive paper and bead on plate welds were then fabricated using a CO₂ continuous laser (Rofin-Sinar 820) with a maximum power of 1.5 kW and a central wavelength of 10.6 μm. The laser beam was focused to a diameter of 0.25 mm on the surface of the plate using a ZnSe lens with a focal length of ~1 mm. Welding parameters included a laser power of 1.0 kW with a scanning velocity of 6 m/min. No filler metal was used. The upper and lower surfaces of the plates were shielded with helium and argon gas, respectively, provided by nozzles with an orifice diameter of 4 mm. The flow rates of the helium and argon were set at 10–20 L/min and 5–15 L/min, respectively.

2.3. Microstructural properties

Specimens for microscopic observation were sectioned and embedded in resin at room temperature and then mechanically polished and chemically etched in an acetic picric solution (5 g picric acid + 5 mL acetic acid + 100 mL ethanol + 10 mL water) for 60 s. Specimens for metallographic analysis were sectioned in planes perpendicular to the direction of the weld and parallel to the weld crown. The sectioned specimens were prepared in accordance with standard metallographic practices, including etching with macrograph and micrograph reagents to enable the identification of the base metal (BM), fusion zone (FZ), and partially melted zone (PMZ). The microstructure of the specimens was characterized (i.e., grain morphology and average grain size) and analyzed

(i.e., precipitate phase and fracture characteristics) using an optical microscope (OM, Olympus BH-2) and a field emission scanning electron microscope (FE-SEM, JSM-6390 LA). The average grain size was determined according to ASTM standard E112 using the linear intercept method. The average grain size values reported in this study are an average of five measurements taken from OM images. The chemical composition and distribution of elements in the specimens were examined using energy dispersive X-ray spectrometry (EDS) and electron probe X-ray microanalysis (EPMA, JEOL JXA-8009R).

2.4. Mechanical properties

2.4.1. Hardness tests

Hardness measurements were performed on the transverse cross-section of the welded specimens using a Vickers hardness tester (Matsuzawa, Seiki MV-1). Hardness measurements were obtained at intervals of 0.6 mm under a load of 300 gf for 15 s. This study investigated the influence of magnesium alloy composition on the hardness in the FZ of welded specimens, as a reflection of differences in hardness in the BM between AZ31 and AZ61 magnesium alloys. This approach enabled researchers to identify a correlation between hardness measurements and the corresponding microstructure (note that the hardness values reported in this study represent the average of five measurements).

2.4.2. Tensile tests

In accordance with the ASTM-E8M standard [24], tensile test specimens with gauge dimensions of 10 mm (diameter) by 17 mm (length) were machined from each weldment in a direction parallel to the extrusion direction of the original alloy plates. The specimens were then polished to obtain a smooth surface. Tensile tests were performed at a constant strain rate of $2.54 \times 10^{-4} \text{ s}^{-1}$ at room temperature using a universal testing machine (Shimadzu AG-10). Surface fractures of the tested specimens were examined using a scanning electron microscope (SEM, JEOL JSM-6500) (note that the tensile strength values reported in this study represent the average value of five measurements).

3. Results and discussion

3.1. Microstructure analysis

Fig. 1 presents OM images illustrating the microstructure of the FZ in AZ31 and AZ61 weldments, respectively. The FZ in the AZ31 weldment is seen to have cellular grains, whereas the bottom of the weld bead comprises columnar grains. By contrast, the FZ of the AZ61 weldment comprises a mixture of cellular and columnar grains and the bottom of the weld bead contains both columnar grains and refined dendrites. A comparison of the PMZ regions of the two weldments demonstrated that the AZ31 weldment did not form a PMZ (see Fig. 1(a)); these specimens formed a PMZ (with a bulk grain structure) only in the AZ61 weldment (see Fig. 1(b)). The images presented in Fig. 1 indicate that the formation of solidified microstructures in the AZ31 and AZ61 weldments depends on the Al content of the original alloy, namely 2.66 wt% and 5.25 wt%, respectively. This finding is consistent with previous studies [10,14,19,25], which reported that the thermal conductivity of magnesium alloys varies as a function of Al content, thereby affecting the supercooling rate and promoting or inhibiting the formation of grains. The change in the FZ microstructure from a cellular grain in the AZ31 weldment to a mixed cellular and columnar grain structure in the AZ61 weldment suggests that a higher Al content enhances recrystallization during cooling.

The average grain size in the FZ of the welds was also measured to take into consideration textural effects (i.e., transverse

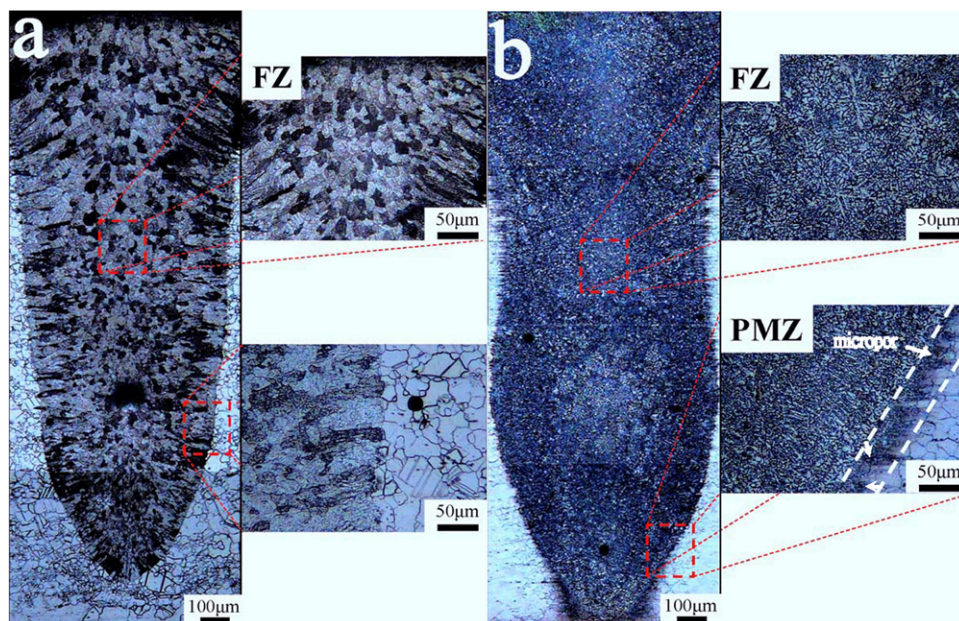


Fig. 1. OM images of microstructures of (a) AZ31 weldment and (b) AZ61 weldment in a direction perpendicular to weld bead.

cross-section), as shown in Fig. 1. The OM images measurements show that the average grain size in the FZ of the AZ31 and AZ61 weldments were approximately $21 \pm 4.7 \mu\text{m}$ and $14 \pm 5.8 \mu\text{m}$, respectively. In other words, the higher Al content of the AZ61 weldment promotes the refinement of grains, which infers that the higher Al content increases the supercooling rate during solidification [26]. Generally, the microstructure, grain size, and composition of elements in the welded specimens depend on heat input conditions [10,14,19,20,26]. This is because weld beads form during the solidification process, and the structure of these depends on the circulation of molten metal, which is influenced by heat input. By contrast, the composition of the metal has a greater influence than heat input on the process of solidification because changes in the composition have a more pronounced influence on temperature gradients. According to the theory of welding metallurgy [23], the mode of solidification can alter grain morphology as the temperature gradient decreases. More specifically, the microstructure in the FZ (comprising mainly cellular grains) and the band region (comprising columnar grains) become increasingly narrow. Measurements show that the average grain sizes in the FZ of the AZ31 and AZ61 weldments were approximately $21 \pm 4.7 \mu\text{m}$ and $14 \pm 5.8 \mu\text{m}$, respectively. In other words, the higher Al content of the AZ61 weldment promotes the refinement of grains, i.e., a smaller average grain size. Therefore, a higher Al content also increases the supercooling rate during solidification.

Fig. 2(a) and (b) presents the SEM/EDX results for the AZ31 and AZ61 weldments, respectively. It can be seen that the FZ in each weldment contains a large quantity of $\beta\text{-Mg}_{17}\text{Al}_{12}$ (identified as circular regions of grey precipitate with a white rim) and $\beta\text{-Mg}_{17}(\text{Al}, \text{Zn})_{12}$ (identified as irregular regions of white precipitate) supersaturated precipitate. It has been reported that these precipitates are the products of a eutectic reaction in the magnesium alloy, prompted by a reduction in the Gibbs free energy [19,25,27,28]. In both weldments, the $\beta\text{-Mg}_{17}\text{Al}_{12}$ and $\beta\text{-Mg}_{17}(\text{Al}, \text{Zn})_{12}$ phases nucleate at grain boundaries. As shown in the figures, the $\beta\text{-Mg}_{17}\text{Al}_{12}$ and $\beta\text{-Mg}_{17}(\text{Al}, \text{Zn})_{12}$ phases in the AZ61 weldment (see Fig. 2(b)) are coarser than those in the AZ31 weldment (see Fig. 2(a)), suggesting that the morphology of the precipitates coarsened and their dimensions increased as a result of supercooling. Furthermore, Zn replaced Al at the saturation limit in the

precipitates. Therefore, the amount of precipitate increased remarkably in the supersaturated $\beta\text{-Mg}_{17}(\text{Al}, \text{Zn})_{12}$ phase. This result is consistent with those of previous studies on the welding of magnesium alloys [14,19,25,26,29]. Surprisingly, Fig. 2(b) shows that the $\beta\text{-Mg}_{17}\text{Al}_{12}$ and $\beta\text{-Mg}_{17}(\text{Al}, \text{Zn})_{12}$ phases in the AZ61 weldment are surrounded by micropores at the bottom of the weld (see Fig. 1(b)). In general, microporosity in weldments is primarily the result of solidification shrinkage, such that the evolution of the dissolved gas occurs in unison and acts collaboratively. The AZ31 weldments fabricated in this study solidified more slowly than the AZ61 weldments (due to their lower Al content), and therefore underwent progressive dendritic feeding during solidification. By contrast, dendritic feeding in the AZ61 weldment is imperfect because of the higher cooling rate, leading to the formation of solidified micropores along the dendritic arms [14,29–32]. It is believed that the formation of micropores in the PMZ of the AZ61 weldment is the result of liquation cracking, caused by the melting of low-temperature grain boundary constituents [22]. Under appropriate stress, cooling rate, and temperature conditions, the micropores grow and coalesce to form voids. Liquation cracking and cracking growth occur when the applied stress exceeds the local tensile strength (i.e., plane tensile stress) at a corresponding temperature. In practice, the local tensile strength and cooling rate both depend on the elemental composition of the welded microstructure, which in turn depends on the composition of the original alloy [23]. Note that the formation of voids reduces the Mg content in the matrix, because each component is transformed into a liquid state during melting and then mixed well through thermal agitation. This implies that the elemental composition may be a dominant factor in phase transformation. As the temperature rapidly drops to room temperature, individual atoms begin solidifying into their preferred crystalline structure. As a result, the atoms of the various elements interfere with one another during the diffusion process. Due to the small volume and rapid heat transfer in the weld bead, the cooling rate is very high, which reduces the time for diffusion. The diffused field of solutes is therefore under a condition of non-equilibrium. These effects shorten the mean free path of the diffusing atoms and as a result, Al and Zn are the primary elements accumulating near the voids. The stress acting at the grain boundaries increases with an increase in cooling rate, which increases the extent of liquation

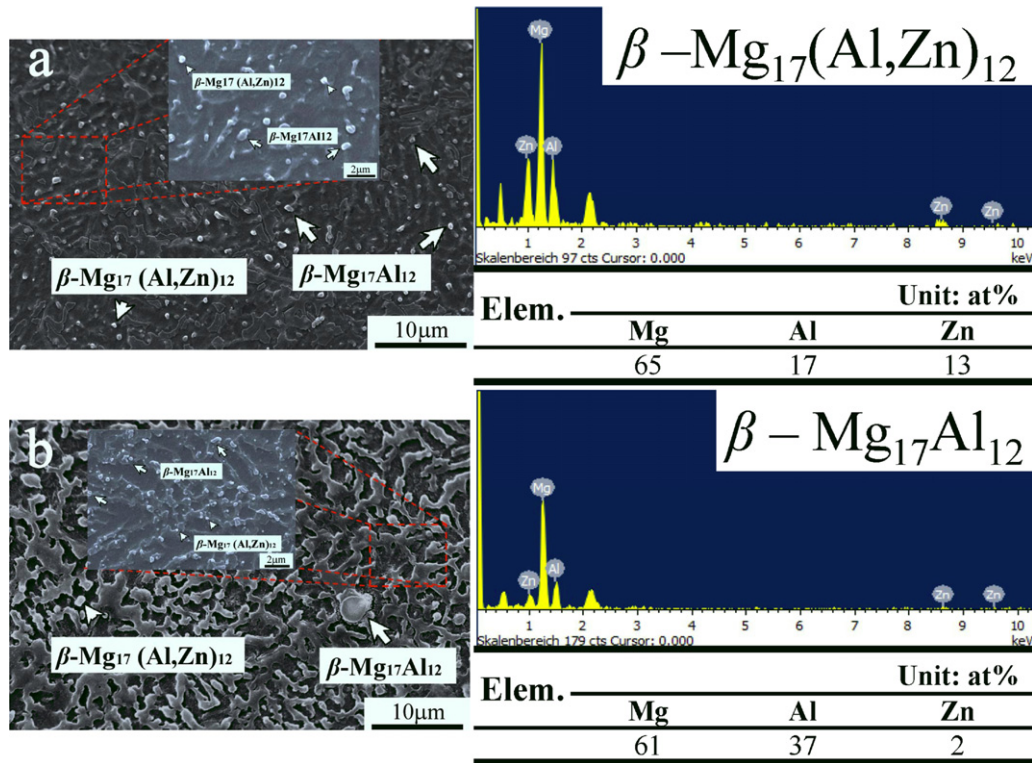


Fig. 2. SEM/EDX showing the distribution of precipitate in the FZ region of (a) AZ31 weldment and (b) AZ61 weldment.

cracking according to the rate at which the structure solidifies. As previously discussed, the PMZ region of the AZ61 weldment cools more rapidly than that of the AZ31 weldment due to its higher Al content. Consequently, liquation cracking is observed in the AZ61 weldment but not in the AZ31 weldment. Furthermore, the FZ of the AZ61 weldment cools more slowly than the PMZ region, leading

to the formation of micropores and voids only in the PMZ region. In addition, the results in Fig. 3 are related to the micropores and voids in the PMZ (i.e., the bottom of a weld bead) of the AZ61 weldment, and suggest that Al and Zn are the primary elements (i.e., Al and Zn contents increased) responsible for the phenomenon of liquation cracking.

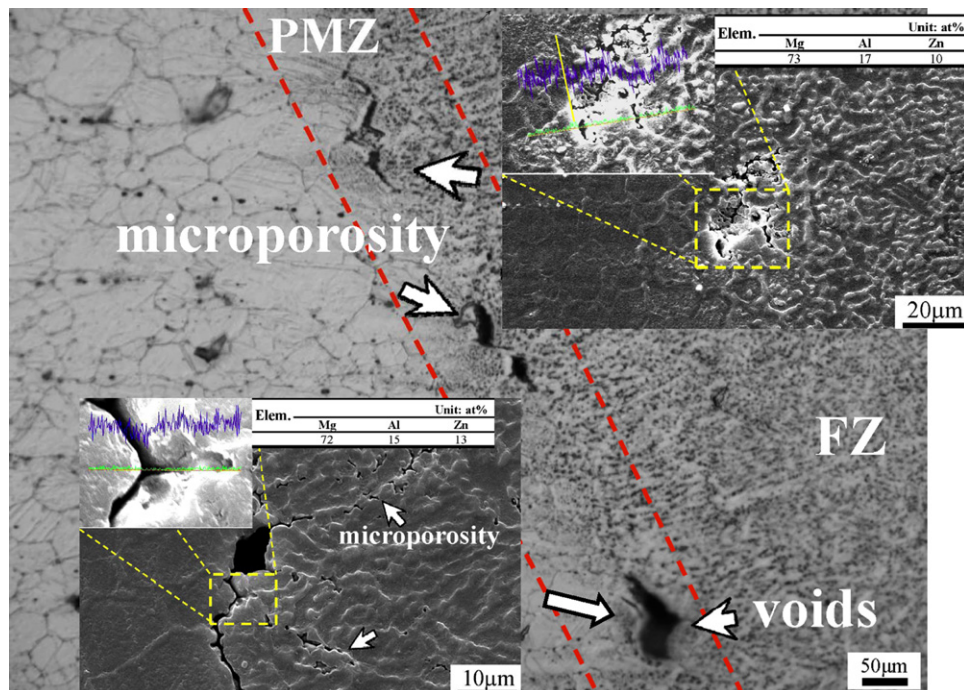


Fig. 3. EPMA elemental mapping for the fracture characteristics of micropores and voids in AZ61 weldment produced by CO₂ laser process.

Table 1
Tensile strength of unwelded and welded AZ31 and AZ61 specimens.

	Tensile Strength (UTS)			Unit: MPa
	AZ31-UW	AZ31-LW	AZ61-UW	AZ61-LW
Ave. value	263 ± 4	247 ± 4	308 ± 3	283 ± 2
	Yield strength (YS)			Unit: MPa
	AZ31-UW	AZ31-LW	AZ61-UW	AZ61-LW
Ave. value	119 ± 6	110 ± 2	153 ± 5	118 ± 6
	Uniform Elongation (%)			
	AZ31-UW	AZ31-LW	AZ61-UW	AZ61-LW
Value	20.1	16.8	20.3	32.7

UW: unwelded weldment; LW: laser weldment.

3.2. Mechanical properties

3.2.1. Hardness properties

Hardness was measured on transverse cross-sections of the welded specimens using a Vickers hardness tester. It was found that the BM regions of the AZ31 and AZ61 weldments have an average hardness of 53 ± 3 HV and 62 ± 2 HV, respectively. This indicates that the CO₂ laser welding process increases the hardness. For both specimens, the maximum hardness was found to occur in the FZ region, i.e., 61 ± 1 HV (AZ31) and 72 ± 2 HV (AZ61). As discussed in previous studies addressing the welding of magnesium alloys [26,33,34], the higher hardness in the FZ region of the weldment is a result of the finer grain structure compared to other regions of the weldment. In addition, precipitates distributed in the matrix are visible in the FZ of the weldment. In [35], it was reported that during the laser welding process, the melted alloy quickly solidifies and cools to room temperature, which reduces the maximum solubility of the Al. As a result, the remaining Al precipitates in supersaturated solutions of β -Mg₁₇Al₁₂ and β -Mg₁₇(Al, Zn)₁₂. However, in our experiment, the content of remaining Al in the AZ61 weldment was found to be much higher, which we infer caused a sharp increase in the precipitation of supersaturated phases. Differences in the precipitate phase in the FZ of each weld can be attributed to differences in the maximum solubility of the Al with which they were produced. The influence of Al content on the supersaturated precipitate phase differs from its influence on hardness; however, this difference is negligible. Therefore, we infer that the primary factor influencing the change in hardness in the FZ is grain refinement.

3.2.2. Tensile properties

Table 1 summarizes the tensile properties of the welded and unwelded AZ31 and AZ61 specimens. It is seen that the ultimate tensile strength (UTS) of the welded AZ31 specimen is approximately 6% lower than that of the unwelded specimen. Similarly, the UTS of the welded AZ61 specimen is approximately 8% lower than that of the unwelded specimen. The UTS values of the AZ61 weldment are approximately 10% higher than those of the AZ31 weldments. By contrast, the UTS values of the unwelded AZ61 specimens are approximately 15% higher than those of the unwelded AZ31 specimens. This UTS analysis shows that there was no significant increase in the tensile strength as a result of welding with AZ31 or AZ61 alloys. These changes in UTS are consistent with previously reported values [14,36]. Thus, we can infer that the tensile strength of the two weldments is insensitive to the Al content in the magnesium alloy. The formation of microstructures and the supersaturated precipitate phase in the FZ of weldments is primarily the result of the melting process and the evolution of metallurgical changes in the weld metal and the weld seam adjacent to the PMZ. There are clear differences between the chemical compositions of

the AZ31 and AZ61 weldments; however, the AZ31 weldments fabricated in this study solidified more slowly than the AZ61 weldments due to their lower Al content, which resulted in coarser grain feeding during solidification. However, the finer grain feeding in the AZ61 weldment was imperfect due to the elevated supercooling rate (see Fig. 1). A cross-section showing the microstructure in the interface area between the FZ and the base metal is presented in Fig. 3. Due to rapid cooling, a fine grained bulk microstructure forms in the PMZ with a near linear orientation toward the center of the weld pool (see Figs. 1 and 3). Due to the large range of temperatures within the PMZ, the material in the magnesium matrix is partially molten. A number of micron scale defects (i.e., micropores) formed within the PMZ during solidification; however, due to their small size, they did not have a detrimental effect on the tensile properties of the weldments. This is due to a diffusion of the base material and weld metal in the FZ, leading to an alteration in the chemical composition in the PMZ. (Note that this change in chemical composition may be the dominant factor associated with the phase transformation. As the temperature rapidly drops to room temperature, atoms begin solidifying into their preferred crystalline structure, during which the atoms of various elements interact with one another. Due to the small volume and rapid heat transfer within the weld bead, the cooling rate is very high, which reduces the diffusion time.) The diffused field of solutes is therefore under a condition of non-equilibrium. These effects shorten the mean free path of the diffusing atoms and as a result, Al and Zn are the primary elements accumulating near the voids. We also compared welded and unwelded AZ31 and AZ61 specimens according to tensile uniform elongation (i.e., ductility). The uniform elongation of the welded AZ31 specimen was found to be approximately 16% lower than that of the unwelded specimen. Similarly, the uniform elongation of the welded AZ61 specimen was found to be approximately 61% higher than that of the unwelded specimen. Moreover, the uniform elongation of the AZ61 weldment is approximately 95% higher than that of the AZ31 weldment (uniform elongation was enhanced). Comparing the yield strength (YS) of welded and unwelded AZ31 and AZ61 specimens demonstrates that the unwelded AZ31 and AZ61 specimens had the highest YS. The YS of the welded AZ31 specimen was 7% lower than that of the unwelded specimen. The YS of the welded AZ61 specimen was more than 23% lower than that of the unwelded specimen. By contrast, the YS of the AZ61 weldments were approximately 7% higher than that of the AZ31 weldment, whereas the YS of the unwelded specimens were approximately 29% higher than that of the welded specimens. These results reveal a significant decrease in YS following welding. It is clear that uniform elongation increased with an increase in Al content in these alloys. Thus, we infer that the uniform elongation of the two weldments is sensitive to the Al content of the magnesium alloy.

3.2.3. Fracture properties

Fig. 4 shows fractures on the surfaces of unwelded and welded AZ31 and AZ61 specimens. Prior to welding, the AZ31 specimen was characterized by ductile fractures (see Fig. 4 (a)). The welded AZ31 is characterized by brittle fracture planes and dimples (see Fig. 4(b)), with the fractures extending deeply into the BM region of the weldment. This is probably due to the formation of a large quantity of β -Mg precipitate (i.e., β -Mg₁₇Al₁₂ and β -Mg₁₇(Al, Zn)₁₂) in the FZ during the solidification process (see Fig. 2), which enhanced the strength of the specimen (perhaps through precipitation strengthening), as demonstrated in the tensile strength tests. These characteristic surface fractures are consistent with those discussed in previous reports [10,14,26]. Prior to welding, the AZ61 specimen was characterized by ductile fractures and dimples, as shown in Fig. 4(c). The welded AZ61 is characterized by brittle fracture planes and dimples (see Fig. 4(d)). It is seen that the

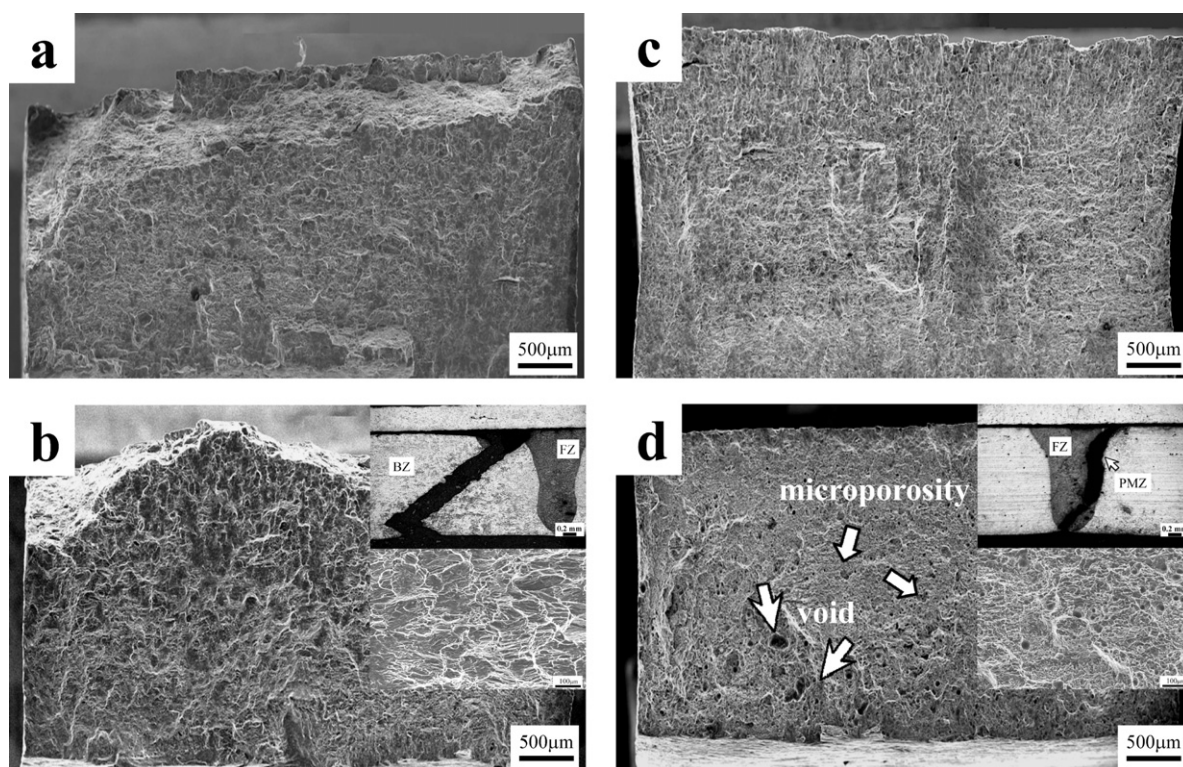


Fig. 4. SEM and OM images of the fractured surfaces of AZ31 and AZ61 weldments: (a) AZ31 specimen prior to welding, (b) AZ31 specimen following welding, (c) AZ61 specimen prior to welding, and (d) AZ61 specimen following welding.

specimen fractured along the shear bands in the PMZ of the weldment. We surmise that the specimen fractured due to the existence of micropores or voids in the bottom region of the weld.

4. Conclusions

1. Differences in the aluminum content of the AZ31 and AZ61 alloys result in a variety of thermal effects that influence the supercooling rate, the formation of precipitates and defects (i.e., micropores and voids), and the solidified grain structure of CO₂ laser weldments.
2. The AZ61 weldments contain micropores and voids in the PMZ region. These defects are believed to be due to the formation of liquation cracks.
3. The CO₂ welding process causes the hardness of both alloys to increase. In both cases, the maximum hardness occurs in the FZ region of the weldment as a result of grain refining.
4. The CO₂ welding process increases the ultimate tensile strength (UTS) of the AZ61 alloy more than that of the AZ31 alloy; however, the difference is not significant. Thus, the tensile strength of the two weldments is insensitive to the Al content of magnesium alloys. By contrast, the uniform elongation in these alloys increased with an increase in Al content. Thus, the uniform elongation of the two weldments is sensitive to the Al content of the magnesium alloys.
5. Fractures in the BM region of AZ31 weldments were caused by the formation of β -Mg precipitate in the FZ, which provides precipitation strengthening. By contrast, the AZ61 weldment fails in the PMZ region of the weldment due to the presence of microstructural defects (i.e., micropores and voids).

References

- [1] Y.J. Chen, Q.D. Wang, J.G. Peng, C.Q. Zhai, W.J. Ding, J. Mater. Process. Technol. 182 (2007) 281–285.
- [2] M.W. Turner, P.L. Crouse, L. Li, A.J.E. Smith, Appl. Surf. Sci. 252 (2006) 4798–4802.
- [3] Y. Karpat, J. Mater. Process. Technol. 211 (2011) 737–749.
- [4] L. Zhang, J.Z. Lu, Y.K. Zhang, K.Y. Luo, J.W. Zhong, C.Y. Cui, D.J. Kong, H.B. Guan, X.M. Qian, Mater. Des. 32 (2011) 480–486.
- [5] J. Yang, F.Z. Cui, I.S. Lee, X. Wang, Surf. Coat. Technol. 205 (2010) 182–187.
- [6] J. Zhang, Q. Yu, Y.Y. Jiang, Q.H. Li, Int. J. Plast. 27 (2011) 768–787.
- [7] Z.W. Shao, Q.C. Le, J.Z. Cui, Z.Q. Zhang, Trans. Nonferrous Met. Soc. China 21 (2011) 1–8.
- [8] X.N. Gu, Y.F. Zheng, Y. Cheng, S.P. Zhong, T.F. Xi, Biomaterials 30 (2009) 484–498.
- [9] L.M. Liu, D.H. Cai, Z.D. Zhang, Scr. Mater. 57 (2008) 695–698.
- [10] L.M. Liu, Z.D. Zhang, G. Song, Y. Shen, Mater. Sci. Eng. A 38 (2007) 649–658.
- [11] J.J. Liu, Y.C. Lin, B.Y. Lin, C.M. Lin, H.L. Tsai, Mater. Des. 35 (2011) 350–357.
- [12] Y.H. Yin, N. Sun, T.H. North, S.S. Hu, Mater. Charact. 61 (2010) 1018–1028.
- [13] Q. Yang, S. Mironov, Y.S. Sato, K. Okamoto, Mater. Sci. Eng. A 527 (2010) 4389–4398.
- [14] C.M. Lin, J.J. Liu, H.L. Tsai, C.M. Cheng, J. Chin. Inst. Eng. 34 (2011) 1013–1023.
- [15] Y. Quan, Z. Chen, X. Gong, Z. Yu, Mater. Sci. Eng. A 496 (2008) 45–51.
- [16] A. Kamel, W.B. Salem, H. Mhiri, L. Georges, A. Michel, Opt. Laser Technol. 40 (2008) 581–588.
- [17] G. Mahendran, V. Balasubramanian, T. Senthilvelan, Mater. Des. 30 (2009) 1240–1244.
- [18] P. Liu, Y.A. Li, H.R. Geng, J. Wang, Mater. Lett. 59 (2005) 2001–2005.
- [19] C. M. Lin, H. L. Tsai, C. L. Lee, S. F. Lee, J. C. Huang, D. S. Chou, J. W. Huang, Int. J. Miner. Metall. Mater., in press.
- [20] D. Min, J. Shen, S.Q. Lai, J. Chen, N. Xu, H. Liu, Opt. Laser Eng. 49 (2011) 89–96.
- [21] C.L. Lee, 'Effects of Welding Heat Input on CO₂ Laser Weldability of AZ31B and AZ61A Magnesium Alloy Extrusion Sheet', Master thesis, National Taiwan University of Science and Technology, Taipei, Taiwan, 2006.
- [22] Z.J. Lu, W.J. Evans, J.D. Parker, S. Birley, Mater. Sci. Eng. A 220 (1996) 1–7.
- [23] S. Kou, J. Miner. Met. Mater. Soc. 55 (2003) 37–42.
- [24] ASTM Standard E8M, ASTM, PA, 2009.
- [25] Y.B. Li, J.F. Huang, H. Cui, K. Tao, K. Zhang, J. Zhang, J. Univ. Sci. Technol. Beijing 15 (2008) 740–746.
- [26] Y. Quan, Z. Chen, Z. Yu, X. Gong, M. Li, Mater. Charact. 59 (2008) 1799–1804.
- [27] F. Heilmann, F. Sommer, B. Predel, Mater. Sci. Eng. A 125 (1990) 249–265.
- [28] C.T. Chi, C.G. Chao, T.F. Liu, C.H. Lee, Scr. Mater. 56 (2007) 733–736.

- [29] S.L. Sin, D. Dubé, R. Tremblay, *Mater. Sci. Technol.* 22 (2006) 1456–1463.
- [30] S.L. Sin, D. Dubé, R. Tremblay, *Mater. Charact.* 59 (2008) 178–187.
- [31] S.G. Lee, G.R. Patel, A.M. Gokhale, A. Sreeranganathan, M.F. Horstemeyer, *Scr. Mater.* 53 (2005) 851–856.
- [32] M. Pastor, H. Zhao, T. DebRoy, *J. Laser Appl.* 12 (2000) 91–100.
- [33] A. Belhadj, J.E. Masse, L. Barrallier, M. Bouhafs, J. Bessrour, *J. Laser Appl.* 12, 56–61.
- [34] Y.J. Quan, Z.H. Chen, X.S. Gong, Z.H. Yu, *Mater. Charact.* 59 (2008) 1491–1497.
- [35] H. Zhao, T. Debroy, *Metall. Mater. Trans. B* 32B (2001) 163–172.
- [36] G. Padmanaban, V. Balasubramanian, *Mater. Des.* 31 (2010) 3724–3732.